

The α -divergence Improves the Entropy Production Estimation via Machine Learning

Euijoon Kwon¹ and Yongjoo Baek^{1,*}

¹*Department of Physics and Astronomy & Center for Theoretical Physics,
Seoul National University, Seoul 08826, Republic of Korea*

(Dated: March 7, 2023)

Recent years have seen a surge of interest in the algorithmic estimation of stochastic entropy production (EP) from the trajectory data via machine learning. A crucial element of such algorithms is the identification of a loss function whose minimization guarantees the accurate EP estimation. In this study, we show that there exists a host of loss functions, namely those implementing a variational representation of the α -divergence, which can be used for the EP estimation. Among these loss functions, the one corresponding to $\alpha = -0.5$ exhibits the most robust performance against strong nonequilibrium driving or slow dynamics, which adversely affects the existing method based on the Kullback-Leibler divergence ($\alpha = 0$). To corroborate our findings, we present an exactly solvable simplification of the EP estimation problem, whose loss function landscape and stochastic properties demonstrate the optimality of $\alpha = -0.5$.

Introduction. — How irreversible does a process look? One may pose this question for two distinct reasons. First, whether a biological process requires energy dissipation is often a subject of much debate [1, 2]. To resolve this issue, it is useful to note that irreversibility suggests energy dissipation. Various hallmarks of irreversibility, such as the breaking of the fluctuation-dissipation theorem [3] and the presence of nonequilibrium probability currents in the phase space [4, 5], have been used to determine whether energy is dissipated. Second, whether a nonequilibrium system allows for an effective equilibrium description is an important issue. For instance, in active matter, despite the energy dissipation at the microscopic level, it has been argued that the large-scale phenomena allows for an effective equilibrium description [6–10]. If we can quantify the irreversibility of an empirical process at various levels of coarse-graining [11, 12], it will provide us with helpful clues as to whether we should look for an effective equilibrium theory for the process.

Based on the framework of stochastic thermodynamics, modern thermodynamics assigns entropy production (EP) to each stochastic trajectory based on its irreversibility [13]. Thus, empirically measuring the irreversibility of a process is closely tied to the problem of estimating EP from sampled trajectories [14–21]. A straightforward approach to the problem is to evaluate the relevant transition probabilities by directly counting the number of trajectory segments, which is called the *plug-in method* [14, 15]. The method, readily applicable to discrete systems, can also be applied to continuous systems through the use of kernel functions [16]. However, while this method is simple and intuitive, it requires a huge ensemble of lengthy trajectories for accurate estimations (*curse of dimensionality*). More recent studies proposed methods based on universal lower bounds of the average EP, such as the thermodynamic uncertainty relations [16–19] and the entropic bound [20].

While these methods do not suffer from the curse of dimensionality and are applicable even to non-stationary processes [19, 20], their accuracy is impaired when the underlying bounds are not tight. Moreover, these methods are applicable only to the estimation of the average EP, not the EP of each trajectory.

Meanwhile, with the advent of machine learning techniques in physics, a novel method for EP estimation using artificial neural networks has been developed [21]. This method, called the Neural Estimator for Entropy Production (NEEP), minimizes the loss function based on a variational representation of the Kullback-Leibler (KL) divergence. Without any presupposed discretization of the phase space and using the rich expressivity of neural networks, the NEEP suffers far less from the complications of the sampling issues and is applicable to a diverse range of stochastic processes [19].

Still, the NEEP has its limits. Its accuracy deteriorates when the nonequilibrium driving is strong or when the dynamics slows down so that the phase space is poorly sampled. In this Letter, we show that the NEEP can be significantly improved by changing the loss function. Toward this purpose, we propose the α -NEEP, which generalizes the NEEP. Instead of the KL divergence, the α -NEEP utilizes the α -divergence, which has been mainly used in the machine learning community [22–25]. We demonstrate that the α -NEEP with $\alpha = -0.5$ shows much more robust performance for a broader range of nonequilibrium driving and sampling quality. This is corroborated by an analytically tractable simplification of the α -NEEP that shows the optimality of $\alpha = -0.5$.

Mathematical framework of the α -NEEP. — Suppose our goal is to estimate the EP of a Markov process in discrete time, \mathbf{x}_t , in a d -dimensional space. Every pair of states, denoted by $\mathbf{x} \equiv (\mathbf{x}_t, \mathbf{x}_{t+1})$, is mapped by the neural network to a real number $r(\mathbf{x})$. The goal of the α -NEEP is to find $r(\mathbf{x})$ that minimizes the loss function

$$\mathcal{L}_\alpha[r] \equiv \left\langle -\frac{r(\mathbf{x})^\alpha - 1}{\alpha} + \frac{q(\mathbf{x}) r(\mathbf{x})^{1+\alpha} - 1}{p(\mathbf{x}) (1 + \alpha)} \right\rangle_{p(\mathbf{x})}, \quad (1)$$

* y.baek@snu.ac.kr

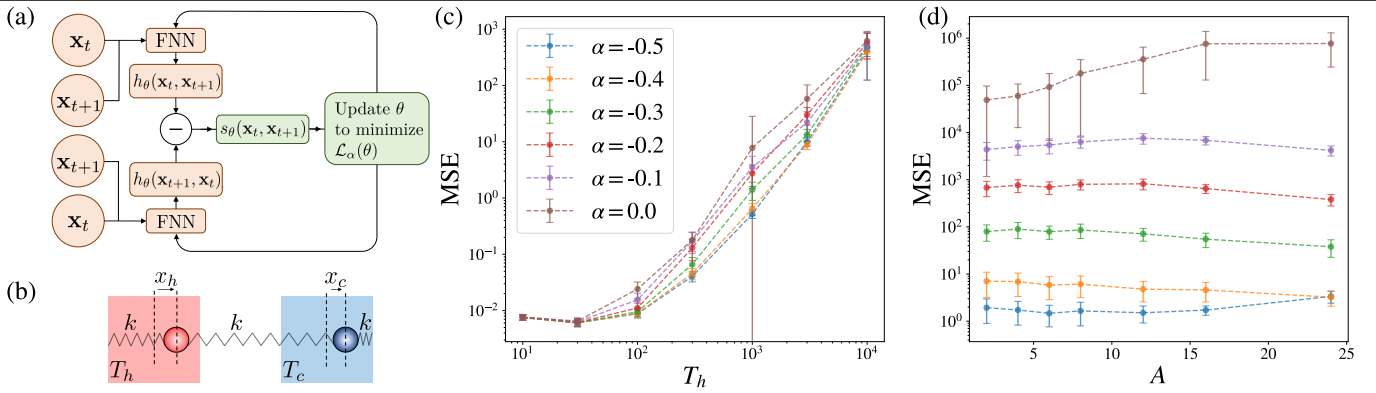


FIG. 1. (a) The architecture of the α -NEEP. (b) An illustration of the two-bead model. (c) The mean square error (MSE) of the EP estimate for the two-bead model for various temperature differences and (d) that of the driven Brownian particle as the potential depth A is varied. The error bars indicate standard deviations obtained from 40 independent trainings. All the other parameters (T_c , γ , and k) are fixed to unity throughout this Letter. Also see Appendix A for more detail about the training procedure. The dashed lines are to guide the eye.

where $p(\mathbf{x})$ and $q(\mathbf{x})$ are probability density functions, $\langle \cdot \rangle_{p(\mathbf{x})}$ denotes the average with respect to the distribution $p(\mathbf{x})$, and α is a real number other than 0 and -1 . See Appendix B for discussions of these two exceptional cases.

It can be rigorously shown (see Appendix B) that $\mathcal{L}_\alpha[r]$ satisfies the inequality

$$\mathcal{L}_\alpha[r] \geq -D_\alpha[p:q] \quad (2)$$

for the α -divergence, a measure of difference between the two distributions $p(\mathbf{x})$ and $q(\mathbf{x})$, defined as

$$D_\alpha[p:q] \equiv \left\langle \frac{[p(\mathbf{x})/q(\mathbf{x})]^\alpha - 1}{\alpha(1+\alpha)} \right\rangle_{p(\mathbf{x})}. \quad (3)$$

Here, $\mathcal{L}_\alpha[r] = -D_\alpha[p:q]$ is achieved if and only if $r(\mathbf{x}) = p(\mathbf{x})/q(\mathbf{x})$ for all \mathbf{x} . In other words, by minimizing $\mathcal{L}_\alpha[r]$ to find $D_\alpha[p:q]$, we also obtain an estimate for the ratio $p(\mathbf{x})/q(\mathbf{x})$. We note that the properties of $\mathcal{L}_\alpha[r]$ used here are also valid for a much more general class of loss functions, as discussed in [22, 23] (also in Appendix B).

Now we show how to estimate the EP using the above properties. First, we identify $p(\mathbf{x})$ and $q(\mathbf{x})$ as the forward and reverse path probabilities $p(\mathbf{x}_t, \mathbf{x}_{t+1})$ and $p(\mathbf{x}_{t+1}, \mathbf{x}_t)$, respectively. The stochastic EP of the transition $\mathbf{x}_t \rightarrow \mathbf{x}_{t+1}$ is given by the log ratio

$$\Delta S(\mathbf{x}_t, \mathbf{x}_{t+1}) = \log \frac{p(\mathbf{x}_t, \mathbf{x}_{t+1})}{p(\mathbf{x}_{t+1}, \mathbf{x}_t)}. \quad (4)$$

Keeping this in mind, we replace $r(\mathbf{x})$ with $e^{s_\theta(\mathbf{x}_t, \mathbf{x}_{t+1})}$ in Eq. (1), where s_θ plays the role of the EP estimator with θ representing the neural network state. Then, the loss

function can be rewritten as

$$\mathcal{L}_\alpha(\theta) = \left\langle -\frac{e^{\alpha s_\theta(\mathbf{x}_t, \mathbf{x}_{t+1})} - 1}{\alpha} + \frac{e^{-(1+\alpha)s_\theta(\mathbf{x}_t, \mathbf{x}_{t+1})} - 1}{1+\alpha} \right\rangle. \quad (5)$$

Here $\langle \cdot \rangle$ denotes the average over all empirical trajectories distributed by $p(\mathbf{x}_t, \mathbf{x}_{t+1})$. This loss function satisfies $\mathcal{L}_{-(1+\alpha)}(\theta) = \mathcal{L}_\alpha(\theta)$, so the α -NEEP is symmetric under the exchange $\alpha \leftrightarrow -(1+\alpha)$. For this reason, through the rest of this Letter, we focus on the regime $-0.5 \leq \alpha \leq 0$ (the regime $\alpha > 0$ leads to very poor performance and is left out). Noting that Eq. (4) implies the antisymmetry $\Delta S(\mathbf{x}_t, \mathbf{x}_{t+1}) = -\Delta S(\mathbf{x}_{t+1}, \mathbf{x}_t)$, we may set the estimator s_θ to be related to the feedforward neural network (FNN) output h_θ as

$$s_\theta(\mathbf{x}_t, \mathbf{x}_{t+1}) = h_\theta(\mathbf{x}_t, \mathbf{x}_{t+1}) - h_\theta(\mathbf{x}_{t+1}, \mathbf{x}_t), \quad (6)$$

so that the neural network focuses on the estimators that satisfy the antisymmetry of EP for more efficient training. The method described so far is schematically illustrated in Fig. 1(a).

We note that the loss function used in the original NEEP [21] is recovered in the limit $\alpha \rightarrow 0$:

$$\begin{aligned} \mathcal{L}_0(\theta) &= \left\langle -1 - s_\theta(\mathbf{x}_t, \mathbf{x}_{t+1}) + e^{-s_\theta(\mathbf{x}_t, \mathbf{x}_{t+1})} \right\rangle \\ &\geq -D_{\text{KL}}[p(\mathbf{x}_t, \mathbf{x}_{t+1}):p(\mathbf{x}_{t+1}, \mathbf{x}_t)]. \end{aligned} \quad (7)$$

Performance of the α -NEEP. — To assess the performance of the α -NEEP, we apply the method to toy models of nonequilibrium systems, namely the two-bead model and the driven Brownian particle.

(i) *The two-bead model.* This model has been used in a number of previous studies as a benchmark for testing EP estimators [4, 16, 18, 21]. The model consists of two 1-d overdamped beads which are connected to each other and to the walls on both sides by identical springs, see

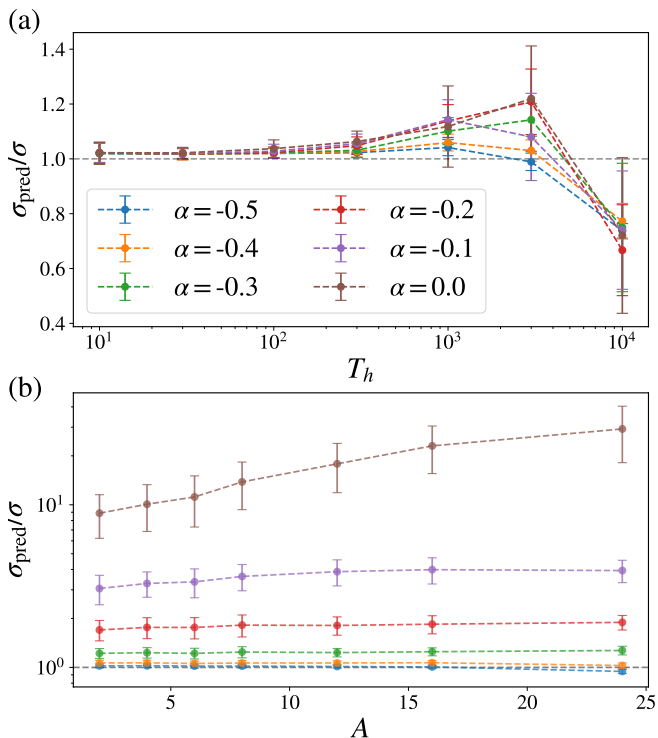


FIG. 2. Ratio between the estimated value σ_{pred} and the true value σ of the average EP for (a) the two-bead model and (b) the driven Brownian particle. Each data point and error bar are obtained from 40 independent trainings.

Fig. 1(b). The beads are in contact with heat baths at temperatures T_h and T_c with $T_h > T_c$. Denoting by x_h (x_c) the bead in contact with the hot (cold) bath, the stochastic equations of motion are given by

$$\dot{x}_h = \frac{k}{\gamma}(-2x_h + x_c) + \sqrt{\frac{2T_h}{\gamma}}\xi_h(t), \quad (8a)$$

$$\dot{x}_c = \frac{k}{\gamma}(-2x_c + x_h) + \sqrt{\frac{2T_c}{\gamma}}\xi_c(t). \quad (8b)$$

Here k is the spring constant, γ the friction coefficient, and $\xi_{h,c}$ the Gaussian thermal noise with zero means and $\langle \xi_h(t)\xi_h(t') \rangle = \langle \xi_c(t)\xi_c(t') \rangle = \delta(t-t')$. For infinitesimal displacements (dx_h, dx_c) , the associated stochastic EP is given by

$$\Delta S = \frac{k}{\gamma} \left[\frac{2x_h - x_c}{T_h} \circ dx_h + \frac{2x_c - x_h}{T_c} \circ dx_c \right] + \Delta S_{\text{sys}}, \quad (9)$$

where \circ denotes the Stratonovich product and ΔS_{sys} the change of the system's Shannon entropy, namely

$$\Delta S_{\text{sys}} = -\ln \frac{p_s(x_h + dx_h, x_c + dx_c)}{p_s(x_h, x_c)} \quad (10)$$

for the steady-state distribution $p_s(x_h, x_c)$. Since the system is fully linear, $p_s(x_h, x_c)$ can be calculated analytically. Thus the EP of this model can be calculated exactly using Eq. (9) and compared with the α -NEEP result.

(ii) *The driven Brownian particle.* As an example of a nonlinear system, we also consider a 1-d overdamped Brownian particle in a periodic potential $U(x) = A \sin x$ driven by a constant force f . The motion of the particle is described by the Langevin equation

$$\dot{x} = f - U'(x) + \sqrt{2T}\xi(t), \quad (11)$$

where $\xi(t)$ is a Gaussian white noise with unit variance. For this model, the stochastic EP associated with the infinitesimal displacement dx is given by

$$\Delta S = \frac{-f dx + U(x + dx) - U(x)}{T} + \Delta S_{\text{sys}}, \quad (12)$$

where $\Delta S_{\text{sys}} = -\ln p_s(x + dx)/p_s(x)$ again denotes the Shannon entropy change for the steady-state distribution $p_s(x)$. Since the system is 1-d, it is straightforward to obtain $p_s(x)$ by numerical integration. Thus, the stochastic EP of this model can also be calculated exactly and compared to the α -NEEP result.

To see how the predicted EP differs from the true EP, we observe the behavior of the mean square error (MSE) $\langle (s_\theta - \Delta S)^2 \rangle$. In Fig. 1(c), we observe that strengthening the nonequilibrium driving (by increasing T_h while keeping $T_c = 1$) tends to impair the EP estimation. This is because a stronger driving makes the reverse trajectories of typical trajectories rarer, lowering the sample quality. Remarkably, the α -NEEP with $\alpha = -0.5$ exhibits the most robust performance. Similarly, in Fig. 1(d), we observe that increasing the amplitude of the periodic potential $U(x)$ results in the increase of the MSE. This may be the consequence of rarer movements across the system as the potential well gets deeper, which means rare trajectories are poorly sampled. Again, the MSE tends to be the smallest for $\alpha = -0.5$.

As an alternative measure of the estimator's performance, we also observe the ratio between the predicted average EP σ_{pred} and the exact average EP σ . The results for the two-bead model are shown in Fig. 2(a), which exhibit two different regimes. As T_h increases, the estimator first overestimates and then underestimates the average EP, with $\sigma_{\text{pred}}/\sigma$ staying closest to 1 for $\alpha = -0.5$. Similarly, in Fig. 2(b), we observe that increasing the potential depth A of the driven Brownian particle leads to an overestimation of the average EP for $\alpha = 0$, while the extent of overestimation stays largely the same for the other cases; in this case, we could not clearly observe the switching of the overestimation regime to the underestimation regime as A is increased further. Nonetheless, again the α -NEEP with $\alpha = -0.5$ gives the best estimation overall.

An exactly solvable one-parameter model. — To understand the observed optimality of $\alpha = -0.5$, we sim-

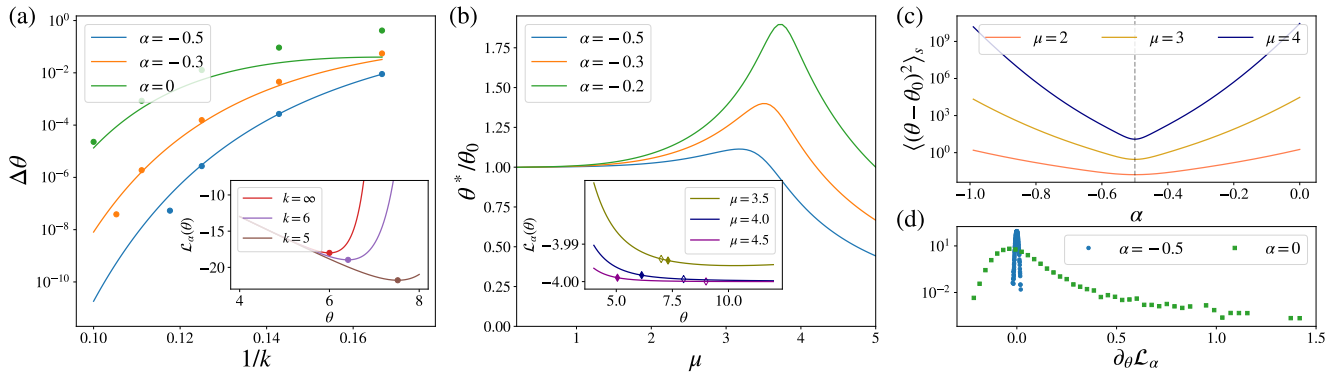


FIG. 3. Performance of the exactly solvable one-parameter model. (a) The shift $\Delta\theta$ of the loss function minimum as a function of the truncation parameter k . The circles are results obtained by numerical minimization, while the solid lines are from the small $1/k$ expansion. (Inset) The loss function landscapes, with the circles indicating the minima. We fixed $\mu = 3$, $\sigma = 1$, and $\alpha = 0$. (b) The ratio of the estimated minimum θ^* to the true minimum θ_0 as the bias μ is varied. The optimal points are calculated using the criterion that the loss function gradient satisfies $|\partial_\theta \mathcal{L}_\alpha(\theta)| < 10^{-3}$ for the first time as θ increases from 0. We fixed $k = 4$ and $\sigma = 1$. (Inset) The loss function landscape. While the open diamonds indicate the true minima θ_0 , the filled diamonds represent the estimated minima θ^* . The parameters $\alpha = -0.5$ and $k = 4$ are fixed. (c) The MSE of θ . The vertical dashed line shows that the error is minimized at $\alpha = -0.5$. (d) The distribution of the loss function gradient $\partial_\theta \mathcal{L}_\alpha$ at the minimum $\theta_0 = 2$ for $\mu = \sigma = 1$.

ply the problem to the density-ratio estimation problem for a 1-d random variable. To be specific, we estimate the log ratio $s(x) \equiv \log p(x)/p(-x)$ given samples drawn from the distribution $p(x)$. It is intuitively clear that this problem is structurally equivalent to EP estimation.

For further simplification, we set

$$p(x) = \begin{cases} \mathcal{N} \exp\left[-\frac{(x-\mu)^2}{2\sigma^2}\right] & \text{for } |x - \mu| \leq k\sigma, \\ 0 & \text{otherwise.} \end{cases} \quad (13)$$

Here \mathcal{N} is a suitable normalization factor, μ the positive mean of the distribution, σ the width of the distribution, and k a positive number truncating the tails of the distribution. While $k = \infty$ corresponds to the perfect sampling of a Gaussian distribution, a finite k corresponds to the case where the tails of the distribution are poorly sampled.

For $k = \infty$, the correct answer to the problem is a linear function $s(x) = \theta_0 x$, where $\theta_0 \equiv 2\mu/\sigma^2$. Thus, for further simplicity, we focus on the *one-parameter model* $s_\theta(x) = \theta x$, which estimates $s(x)$ using only a single parameter θ . For this problem, the suitable loss function is obtained as an analog of Eq. (5):

$$\mathcal{L}_\alpha(\theta) = \left\langle -\frac{(1+\alpha)e^{\alpha\theta x} - 1}{\alpha} + e^{-(1+\alpha)\theta x} \right\rangle_{p(x)}. \quad (14)$$

If k is large but finite, the minimum of this loss function shifts to $\theta_0 + \Delta\theta$, where $\Delta\theta$ can be expanded to the leading orders in $1/k$:

$$\Delta\theta \sim \exp\left[-\frac{k^2}{2} + \frac{2\mu}{\sigma} \left(\left|\alpha + \frac{1}{2}\right| + \frac{1}{2}\right)k\right]. \quad (15)$$

This clearly shows that $\alpha = -0.5$ gives the least shift $\Delta\theta$, as also illustrated by various results shown in Fig. 3.

In Fig. 3(a), we show that the shift of the minimum $\Delta\theta$ tends to increase as the tail sampling becomes poorer (*i.e.*, k decreases). The landscapes of the loss function $\mathcal{L}_\alpha(\theta)$, shown in the inset of Fig. 3(a), also confirm this observation. The increase of the error with the potential depth A in Figs. 1(d) and 2(b) may primarily be due to the same effect.

In Fig. 3(b), we plot the ratio between the estimated minimum θ^* and the true minimum θ_0 as a function of the mean μ , which is an analog of the nonequilibrium driving. We note that here θ^* is the lowest value of θ at which the slope of the loss function becomes less than 10^{-3} . We observe that an overestimation regime ($\theta^*/\theta_0 > 1$) crosses over to an underestimation regime ($\theta^*/\theta_0 < 1$) as μ grows. This is in striking agreement with the trends shown in Fig. 2(a). The reason why θ^* underestimates θ_0 for large μ can be understood by the flattened loss function landscapes shown in the inset of Fig. 3(b). In this regime, the dynamics of θ (starting from $\theta = 0$) slows down, ending up at a value (filled diamonds) even lower than θ_0 (empty diamonds). This effect is due to the samples with $x < 0$ vanishing when μ is too large.

The one-parameter model also allows us to examine the effects of the finite mini-batch size M . While the ideal loss function is given in Eq. (14), the loss function used in the actual training looks like

$$\mathcal{L}_\alpha(\theta; M) = \frac{1}{M} \sum_i \left[-\frac{(1+\alpha)e^{\alpha\theta X_i} - 1}{\alpha} + e^{-(1+\alpha)\theta X_i} \right], \quad (16)$$

where X_1, \dots, X_M are i.i.d. Gaussian random variables of mean μ and variance σ^2 . When M is large and finite,

using the central limit theorem (CLT), the gradient of this loss function can be approximated as [26, 27]

$$\left. \frac{\partial \mathcal{L}_\alpha}{\partial \theta} \right|_{\theta=\theta_t} = \bar{K}(\theta_t - \theta_0) + \sqrt{\frac{\Lambda}{M}} N_t + o(M^{-1/2}), \quad (17)$$

where $\theta_0 = \operatorname{argmin}(\langle \mathcal{L}_\alpha(\theta) \rangle)$, $\bar{K} = \partial_\theta^2 \langle \mathcal{L}_\alpha \rangle|_{\theta=\theta_0}$, and $\Lambda = \operatorname{Var}[\partial_\theta \mathcal{L}_\alpha|_{\theta=\theta_0, M=1}]$. When the stochastic gradient descent $\theta_{t+1} = \theta_t - \lambda(\partial \mathcal{L}_\alpha / \partial \theta)|_{\theta=\theta_t}$ reaches the steady state, the MSE of θ is given by

$$\langle (\theta - \theta_0)^2 \rangle_s = \frac{\lambda \Lambda}{M \bar{K} (2 - \lambda \bar{K})} + o(M^{-1}). \quad (18)$$

This leading-order behavior is shown in Fig. 3(c) for various values of μ . For all cases, the MSE of θ is minimized at $\alpha = -0.5$, which is consistent with the smallest error bars observed at $\alpha = -0.5$ in Figs. 1 and 2. Hence, $\alpha = -0.5$ yields the most consistent EP estimator.

Direct measurements of the loss function gradient at the minimum also confirm the above result. As shown in Fig. 3(d), the gradient $\partial_\theta \mathcal{L}_\alpha$ is far more broadly distributed for $\alpha = 0$ than for $\alpha = -0.5$. Moreover, due to the subleading effects (beyond the CLT) of finite M , the gradient for $\alpha = 0$ features a large skewness. These show that the training dynamics for the original NEEP

($\alpha = 0$) tends to be far more volatile and unstable than for the α -NEEP with $\alpha = -0.5$.

Summary and outlook. — We proposed the α -NEEP, a generalization of the NEEP for estimating the steady-state EP at the trajectory level. Comparing the performance for various values of α , we found that $\alpha = -0.5$ is the best in the following regards: (i) it is the most robust against poor sampling caused by strong nonequilibrium driving or deep potential wells; (ii) it gives the most consistent EP estimate with smallest error bars. We also demonstrated the optimality of $\alpha = -0.5$ using a simplification of the original EP estimation problem, whose loss function landscape and relaxation properties are analytically tractable. The α -NEEP thus provides a powerful method for estimating the EP for much broader range of the nonequilibrium driving force and the time scale of dynamics. Identification of even better loss functions and optimization of other hyperparameters (network size, number of iterations, etc.) are left as future works. It would also be interesting to apply the α -NEEP to estimations of the EP of the Brownian movies [28] and stochastic systems with odd-parity variables [29], which have been studied using the original NEEP method.

Acknowledgments. — This work was supported by the National Research Foundation of Korea Grant funded by the Korean Government (NRF-2020R1C1C101443613). EK and YB also thank Junghyo Jo and Sangyun Lee for helpful comments.

Appendix A: Training details

We always use the fully connected network (FCN) with three hidden layers, with each layer composed of 512 nodes. Each training dataset consists of 10^6 trajectories. The neural network parameters are updated using the ReLU activation function and the Adam optimizer. The learning rate is fixed to 10^{-5} and the weight decay is fixed to 5×10^{-5} . We halt the training after 10,000 iterations, except for the results shown in Figs. S3 and S4. All trainings are done on PyTorch with NVIDIA GeForce RTX 3090.

In Fig. 1(c, d), each mini-batch consists of 10^4 trajectories. In Fig. 2(a, b), each mini-batch consists of 10^5 trajectories.

Appendix B: Density ratio estimation using f -divergence

Consider a convex, twice-differentiable real-valued function $f(u)$. Then, the inequality

$$-pf'(u) + q(uf'(u) - f(u)) \geq -qf(p/q) \quad (\text{B1})$$

holds. We can verify this by differentiating the lhs with respect to u , which yields $f''(u)(-p + qu)$. Thus the lhs has a local minimum at $u = p/q$, and this is the only local minimum since f is convex. In addition, the second derivative of the lhs at $u = p/q$ equals $qf''(p/q)$, which is positive by the convexity. This proves the inequality (B1). Using this, we

can design a loss function whose minimum is equal to the negative f -divergence between two probability distributions $p(\mathbf{x})$ and $q(\mathbf{x})$. To be specific, for any function $r(\mathbf{x})$, we define

$$\begin{aligned}\mathcal{L}_f[r] &= \left\langle -f'(r(\mathbf{x})) + \frac{q(\mathbf{x})}{p(\mathbf{x})} \{r(\mathbf{x})f'(r(\mathbf{x})) - f(r(\mathbf{x}))\} \right\rangle_{p(\mathbf{x})} \\ &= \int d^{2d}\mathbf{x} [-p(\mathbf{x})f'(r(\mathbf{x})) + q(\mathbf{x}) \{r(\mathbf{x})f'(r(\mathbf{x})) - f(r(\mathbf{x}))\}].\end{aligned}\quad (\text{B2})$$

Using Eq. (B2), we conclude that

$$\mathcal{L}_f[r] \geq - \int d^{2d}\mathbf{x} q(\mathbf{x}) f\left(\frac{p(\mathbf{x})}{q(\mathbf{x})}\right) = -D_f[p:q], \quad (\text{B3})$$

where $D_f[p:q]$ is the f -divergence between the distributions $p(\mathbf{x})$ and $q(\mathbf{x})$, and the equality holds if and only if $r(\mathbf{x}) = p(\mathbf{x})/q(\mathbf{x})$ for all \mathbf{x} . By minimizing $\mathcal{L}_f[r]$, we can estimate $p(\mathbf{x})/q(\mathbf{x})$ as well as $D_f[p:q]$.

The loss function \mathcal{L}_α and the associated α -divergence discussed in the main text are obtained by choosing the function f to be

$$f_\alpha(u) = \begin{cases} \frac{u^{1+\alpha} - (1+\alpha)u + \alpha}{\alpha(1+\alpha)} & \text{for } \alpha \neq 0, -1, \\ u \log u & \text{for } \alpha = 0, \\ \log u + 1 - u & \text{for } \alpha = -1. \end{cases} \quad (\text{B4})$$

Note that $f_0(u) = \lim_{\alpha \rightarrow 0} f_\alpha(u)$ and $f_{-1}(u) = \lim_{\alpha \rightarrow -1} f_\alpha(u)$. It is straightforward to obtain Eq. 5 of the main text and its extensions to the cases $\alpha = 0$ and $\alpha = -1$ from this choice.

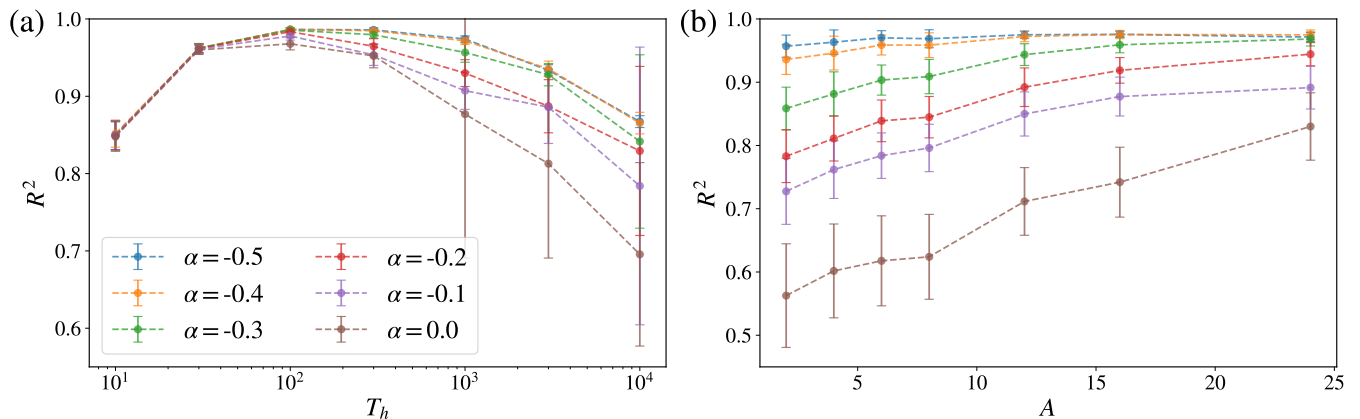


FIG. 4. Coefficient of determination R^2 . 10^4 trajectories are used for each mini-batch, and error bars indicate the standard deviations obtained from 40 independent trainings. (a) For the two-bead model, R^2 exhibits a non-monotonic behavior as a function of T_h (while $T_c = 1$). The decrease of R^2 near equilibrium ($T_h = 1$) is due to the overfitting phenomenon, which disrupts the linear relationship between s_θ and ΔS . (b) For the driven Brownian particle, R^2 always increases with A . This may seem contradictory to how the MSE increases with A in Fig. 1(d) of the main text. Indeed, higher R^2 only means that there is a good linear relationship between the EP estimate s_θ and the true EP ΔS , not that s_θ and ΔS are close to each other. This clearly shows that R^2 is not an adequate measure of the performance of EP estimators.

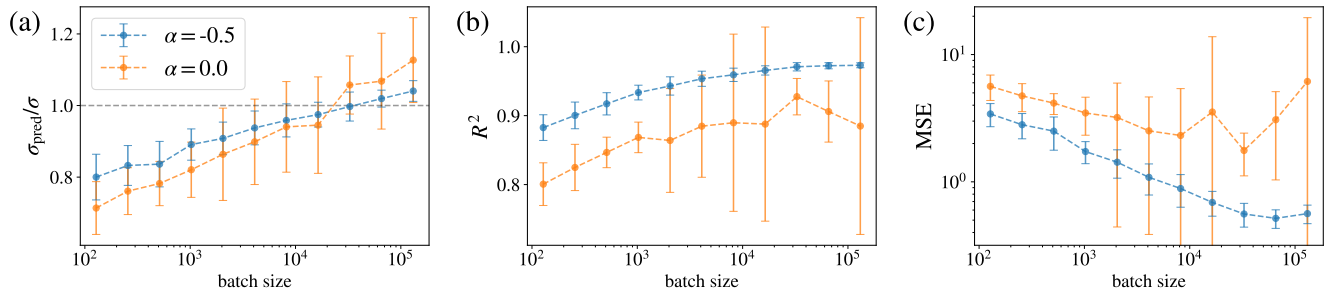


FIG. 5. Effects of the mini-batch size on the performance of the α -NEEP for the two-bead model with $T_h = 1000$. We use three different measures of the performance. Error bars indicate the standard deviations obtained from 40 independent trainings. For small mini-batches, the highly skewed distribution of the stochastic gradient causes underestimation of the EP. For large mini-batches, the distortion of the loss function landscape stemming from poor sampling leads to overestimation of the EP. All three measures confirm the superiority of $\alpha = -0.5$ to $\alpha = 0$.

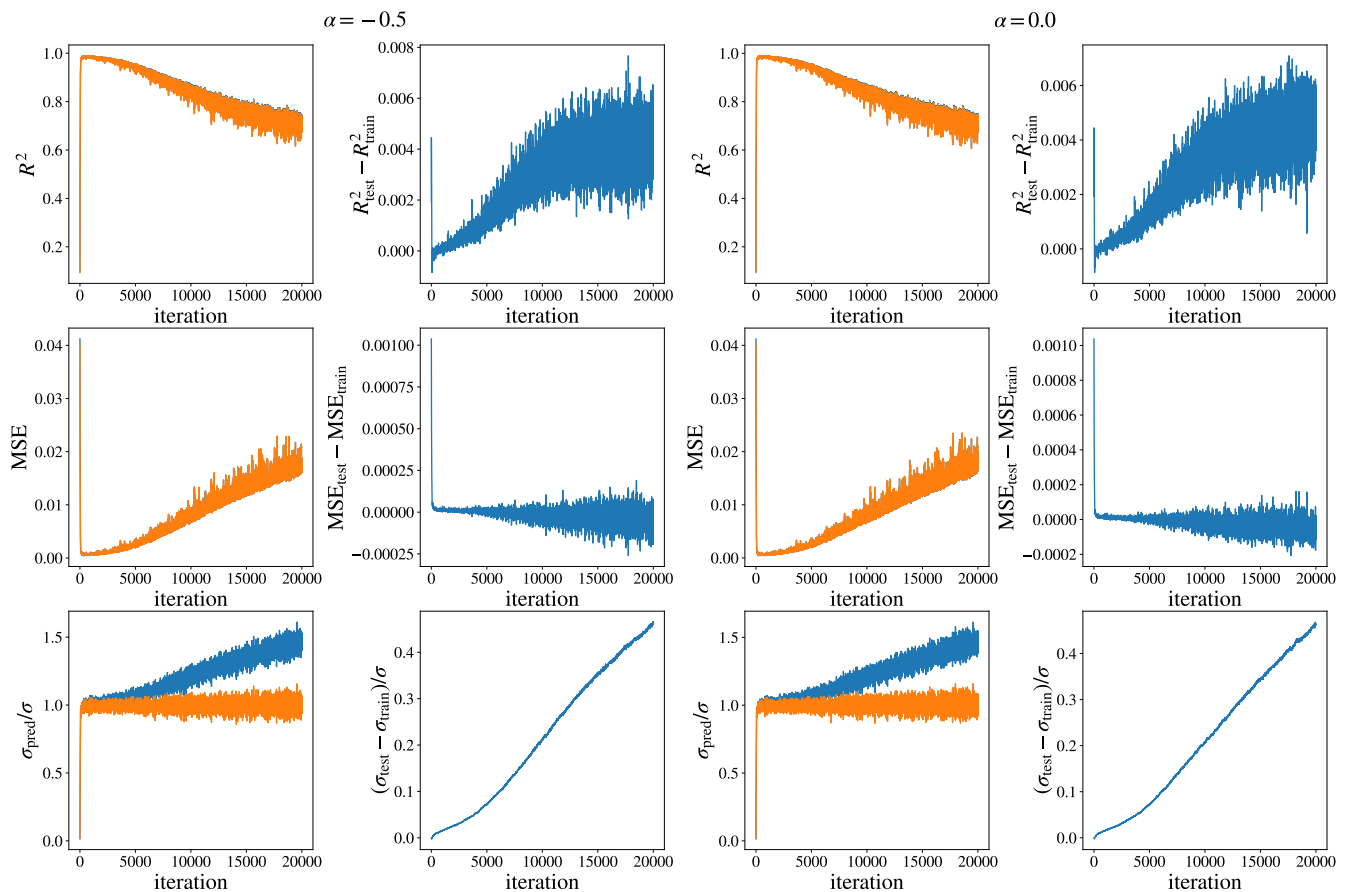


FIG. 6. Training dynamics of the α -NEEP for the two-bead model at $T_h = 10$. Each mini-batch consists of 10^5 trajectories. The first (last) two columns show the dynamics for $\alpha = -0.5$ ($\alpha = 0$). The first and the third columns show the three different measures of performance for the training dataset and the test dataset. The second and the fourth columns show the difference between the corresponding measures obtained for two datasets. We note that the test dataset is independently generated. The overfitting phenomena are manifest from the decrease of R^2 and the increase of the MSE towards the end of the training. Interestingly, overfitting leads to an overestimation of the average EP only for the training dataset. We also note that the value of α is largely irrelevant to the extent of overfitting. This phenomenon can be explained as follows. Near equilibrium, the neural network swiftly reaches the loss function minimum. However, as the training continues, the neural network starts to see the detailed fluctuations of the training dataset. This makes the functional form of s_θ very rough, leading to the increase of the MSE and R^2 for both datasets. But while the neural network now believes all trajectories in the training dataset to be highly irreversible and assigns high EP to them, the EP assigned to the trajectories in the test dataset stay unbiased.

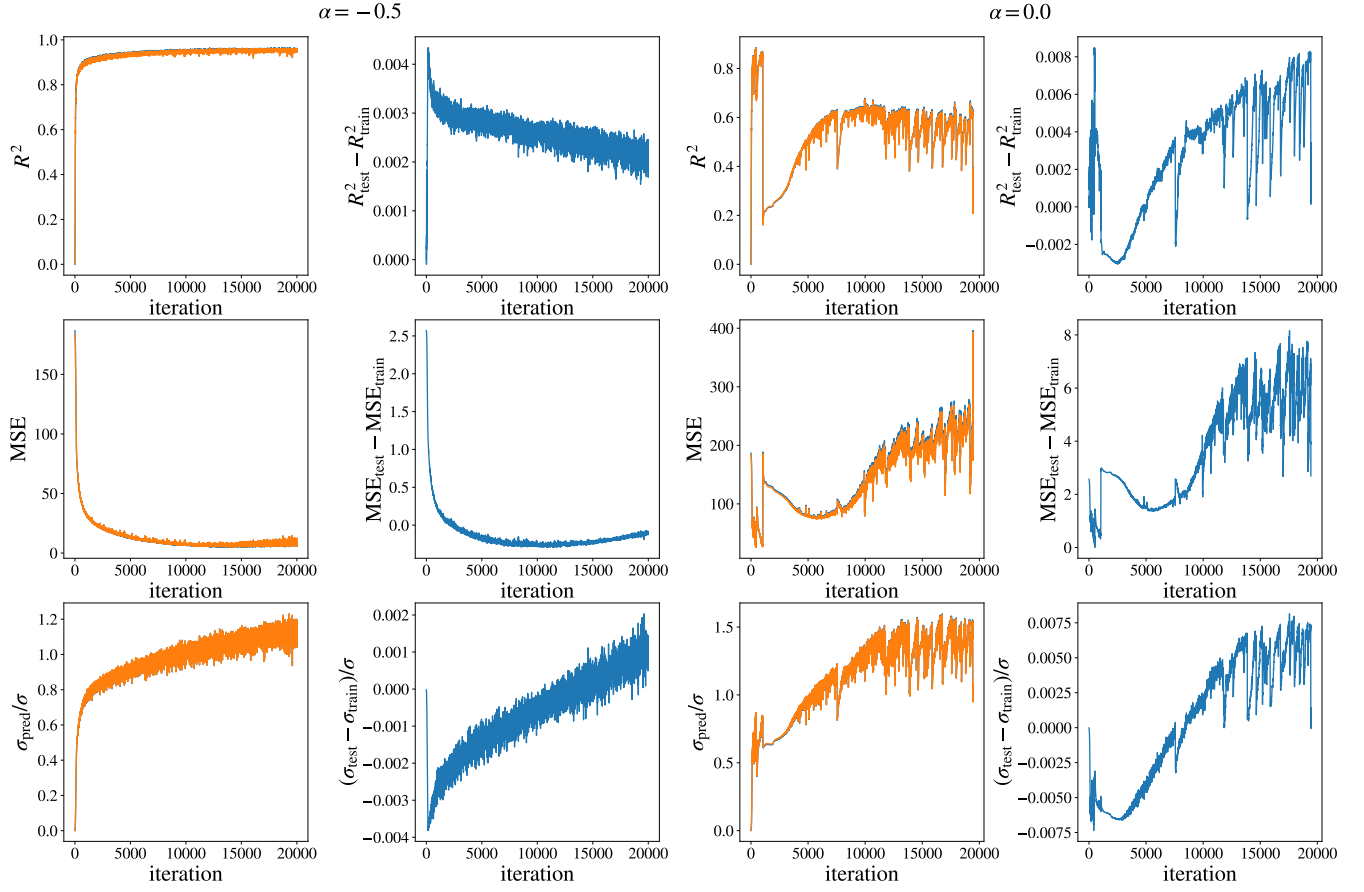


FIG. 7. Training dynamics of the α -NEEP for the two-bead model at $T_h = 3000$. Each mini-batch consists of 10^5 trajectories. The subfigures are organized in exactly the same way as in Fig. S3. In this case, the overfitting effects are not pronounced, and the differences between the training and the test datasets are very small. Note that $\alpha = 0$ exhibits strong noise effects, which is in agreement with the gradient distribution shown in Fig. 3(d) of the main text.

-
- [1] C. P. Brangwynne, G. H. Koenderink, F. C. MacKintosh, and D. A. Weitz, *J. Cell Biol.* **183**, 583 (2008).
- [2] S. C. Weber, A. J. Spakowitz, and J. A. Theriot, *Proc. Natl. Acad. Sci.* **109**, 7338 (2012).
- [3] D. Mizuno, C. Tardin, C. F. Schmidt, and F. C. MacKintosh, *Science* **315**, 370 (2007).
- [4] C. Battle, C. P. Broedersz, N. Fakhri, V. F. Geyer, J. Howard, C. F. Schmidt, and F. C. MacKintosh, *Science* **352**, 604 (2016).
- [5] J. Gladrow, N. Fakhri, F. C. MacKintosh, C. F. Schmidt, and C. P. Broedersz, *Phys. Rev. Lett.* **116**, 248301 (2016).
- [6] J. Tailleur and M. E. Cates, *Phys. Rev. Lett.* **100**, 218103 (2008).
- [7] T. Speck, J. Bialké, A. M. Menzel, and H. Löwen, *Phys. Rev. Lett.* **112**, 218304 (2014).
- [8] S. C. Takatori, W. Yan, and J. F. Brady, *Phys. Rev. Lett.* **113**, 028103 (2014).
- [9] T. F. F. Farage, P. Krinninger, and J. M. Brader, *Phys. Rev. E* **91**, 042310 (2015).
- [10] A. P. Solon, J. Stenhammar, M. E. Cates, Y. Kafri, and J. Tailleur, *Phys. Rev. E* **97**, 020602(R) (2018).
- [11] E. Fodor, C. Nardini, M. E. Cates, J. Tailleur, P. Visco, and F. van Wijland, *Phys. Rev. Lett.* **117**, 038103 (2016).
- [12] C. Nardini, E. Fodor, E. Tjhung, F. van Wijland, J. Tailleur, and M. E. Cates, *Phys. Rev. X* **7**, 021007 (2017).
- [13] U. Seifert, *Rep. Prog. Phys.* **75**, 126001 (2012).
- [14] E. Roldán and J. M. R. Parrondo, *Phys. Rev. Lett.* **105**, 150607 (2010).
- [15] E. Roldán and J. M. R. Parrondo, *Phys. Rev. E* **85**, 031129 (2012).
- [16] J. Li, J. M. Horowitz, T. R. Gingrich, and N. Fakhri, *Nat. Commun.* **10**, 1666 (2019).
- [17] T. Van Vu, V. T. Vo, and Y. Hasegawa, *Phys. Rev. E* **101**, 042138 (2020).
- [18] S. Otsubo, S. Ito, A. Dechant, and T. Sagawa, *Phys. Rev. E* **101**, 062106 (2020).
- [19] S. Otsubo, S. K. Manikandan, T. Sagawa, and S. Krishnamurthy, *Commun. Phys.* **5**, 11 (2022).
- [20] S. Lee, D.-K. Kim, J.-M. Park, W. K. Kim, H. Park, and J. S. Lee, “Multidimensional entropic bound: Estimator of entropy production for general langevin dynamics with an arbitrary time-dependent protocol,” [arXiv:2207.05961](https://arxiv.org/abs/2207.05961) [[cond-mat.stat-mech](https://arxiv.org/abs/2207.05961)].
- [21] D.-K. Kim, Y. Bae, S. Lee, and H. Jeong, *Phys. Rev. Lett.* **125**, 140604 (2020).
- [22] A. Basu, I. R. Harris, N. L. Hjort, and M. C. Jones, *Biometrika* **85**, 549 (1998).
- [23] M. Sugiyama, T. Suzuki, and T. Kanamori, *Density ratio estimation in machine learning* (Cambridge University Press, 2012).
- [24] S. Nowozin, B. Cseke, and R. Tomioka, in *Proceedings of the 30th International Conference on Neural Information Processing Systems* (2016) pp. 271–279.
- [25] M. I. Belghazi, A. Baratin, S. Rajeshwar, S. Ozair, Y. Bengio, A. Courville, and D. Hjelm, in *International Conference on Machine Learning* (PMLR, 2018) pp. 531–540.
- [26] Q. Li, C. Tai, and W. E, in *Proceedings of the 34th International Conference on Machine Learning*, Proceedings of Machine Learning Research, Vol. 70, edited by D. Precup and Y. W. Teh (PMLR, 2017) pp. 2101–2110.
- [27] P. Chaudhari and S. Soatto, in *2018 Information Theory and Applications Workshop (ITA)* (IEEE, 2018) pp. 1–10.
- [28] Y. Bae, D.-K. Kim, and H. Jeong, *Phys. Rev. Res.* **4**, 033094 (2022).
- [29] D.-K. Kim, S. Lee, and H. Jeong, *Phys. Rev. Res.* **4**, 023051 (2022).